Forschung im Ingenieurwesen (2025)89:22
https://doi.org/10.1007/s10010-025-00778-2

ORIGINALARBEITEN/ORIGINALS

Quantification of smearing risk for tapered roller bearings in wind turbine gearboxes during grid faults

Emircan Yazici[1] · Georg Jacobs[1] · Julian Röder[1] · Julian Mogk[1] · Patrick Wingertszahn[2] · Oliver Koch[2]

Received: 19 September 2024 / Accepted: 29 January 2025

Abstract

Wind turbine (WT) gearbox damage negatively impact the levelized cost of energy due to the costs for maintenance and repair. In 70% of the cases, rolling bearing damage are the cause of WT gearbox failures. Rolling bearings often fail far before their designed service life. Especially the bearings on the high-speed-shaft (HSS) of the WT gearbox are prone to failure. One driver for bearing damage are critical loads that are not sufficiently included in the design process yet, e.g. loads resulting from grid faults. Grid faults induce significant generator torque excitations in doubly-fed induction generator wind turbines which lead to transient changes in the loading and rotational speed of the gearbox bearings. Typically, cylindrical roller bearings (CRB) and tapered roller bearings (TRB) are used on the HSS. For CRBs, it was already shown in previous publications that the smearing risk is significantly increased in the event of grid faults. For TRBs, there is no such investigation yet. TRBs are often used as the fixed bearing in an adjusted bearing arrangement on the HSS. The preloading of the arrangement significantly influences the bearing kinematics and the risk of damage. Thus, this paper investigates the smearing risk for TRBs in WT gearboxes during grid faults, considering different preloads of the bearings. It is shown that the smearing risk for the TRBs on the HSS of a research nacelle during grid faults is 72% higher than during rated operation for the reference preload distance of 0 µm. Increasing the preload distance to 370 µm leads to a significant decrease in the smearing risk by 55% for the rated operation and by 86% during the grid fault compared to the reference. However, increasing the preload also increases the fatigue loads and thus decreases the fatigue lifetime. Consequently, there has to be a multifactorial design optimization of the TRB arrangement and the different damage criteria to derive the optimal preload.

Abbreviations

CRB	Cylindrical roller bearing
FPI	Frictional power intensity
GS	Generator-side
HSS	High-speed-shaft
LaMBDA	Lager Mehrkörper Berechnung und Dynamik Analyse
LCOE	Levelized cost of electricity
MBS	Multibody simulation
RS	Rotor-side
TRB	Tapered roller bearing
WT	Wind turbine

Formulas

δ [µm]	Axial clearance
Δu [m/s]	Relative speed of contact partners
μ [–]	Friction coefficient
A [m²]	Contact area
a [m]	Semi-axes of ellipse
b [m]	Semi-axes of ellipse
F_N [N]	Normal force in contact
F_{rad} [N]	Radial force
F_T [N]	Tangential force in contact
n_{IR} [rad/s]	Inner ring speed
$n_{WK,kin}$ [rad/s]	Kinematic roller element speed
P [W]	Power
p [Pa]	Contact pressure
P_{limit} [Pa]	Maximum fatigue pressure
t [s]	Time

✉ Emircan Yazici
emircan.yazici@cwd.rwth-aachen.de

[1] Center for Wind Power Drives, RWTH Aachen University, Aachen, Germany

[2] Chair of Machine Elements, Gears and Tribology, RPTU Kaiserslautern-Landau, Kaiserslautern, Germany

Published online: 19 February 2025

Quantifizierung des Risikos gegenüber Anschmierung bei Kegelrollenlagern in Getrieben von Windenergieanlagen bei Netzfehler

Zusammenfassung

Getriebeschäden bei Windenergieanlagen (WEA) führen aufgrund der Wartungs- und Reparaturkosten zu höheren Stromgestehungskosten. In 70 % der Fälle sind frühzeitige Ausfälle der Wälzlager, insbesondere auf der High-Speed-Shaft (HSS), Ursache für diese Schäden. Eine Ursache für diese Ausfälle sind kritische Lasten z. B. durch Netzfehler, die bei der Auslegung nicht ausreichend berücksichtigt werden. Netzfehler induzieren in WEA mit doppelt gespeistem Asynchrongenerator große Drehmomentschwankungen, die zu dynamischen Lasten und Geschwindigkeiten der Wälzlager führen. In der Regel werden Zylinderrollenlager und Kegelrollenlager (TRB, engl.:"tapered roller bearing") auf der HSS eingesetzt. Für Zylinderrollenlager wurde bereits in früheren Veröffentlichungen gezeigt, dass das Risiko gegenüber Anschmierung bei Netzfehler erhöht ist. Für TRB liegen keine Untersuchungen vor. TRBs werden häufig als angestellte Festlager auf der HSS eingesetzt. Die Vorspannung der Lagerstelle hat großen Einfluss auf die Lagerdynamik. Daher wird in dieser Veröffentlichung unter Berücksichtigung der Vorspannung das Risiko gegenüber Anschmierung für TRB in WEA-Getrieben bei Netzfehler untersucht. Es wird gezeigt, dass das Risiko gegenüber Anschmierung von TRBs auf der HSS einer Forschungsgondel bei Netzfehler um 72 % höher ist als im Nennbetrieb. Eine Erhöhung des Vorspannweges auf 370 µm führt zu einer Verringerung des Risikos um 55 % während des Nennbetriebs und um 86 % während des Netzfehlers. Die Erhöhung der Vorspannung führt jedoch zu erhöhten Ermüdungslasten und damit zu einer Verringerung der Ermüdungslebensdauer. Folglich ist eine multifaktorielle Designoptimierung der Lagerstelle unter Berücksichtigung verschiedener Schadenskriterien erforderlich, um die optimale Vorspannung zu ermitteln.

1 Motivation

Wind energy is a key driver in the development of a climate-neutral energy supply. In order to further increase the share of wind energy, a reduction of the levelized cost of electricity (LCOE) is necessary [1]. The LCOE is negatively affected by failures and downtimes of WTs. The longest downtimes are caused by gearbox damage [2]. One of the most frequently failing components of WT gearboxes are the rolling bearings of the HSS. High speeds in combination with dynamic loads result in bearing dynamics that make the rolling bearings prone to slip-induced damage such as smearing [3]. Smearing is based on adhesive wear which is caused by high pressure and high slip. High pressure and slip are induced, among others, by generator torque excitations. Torque excitations in the generator can be caused by electrical faults such as grid faults [4]. The torque excitations cause the gear forces to fluctuate, which can result in high pressures and high slippage in the bearings [5]. Typically, CRBs and TRBs are used on the HSS. Previous studies showed that the risk of damage for CRBs increases during grid faults [6]. For TRBs there has not been such an investigation yet. Therefore, this paper quantifies the risk of smearing for TRBs on the HSS of a WT gearbox during grid faults. Slip in TRBs can be counteracted by preloading. Conversely, adjusting the preload significantly influences the rolling bearing dynamics and performance.

2 Influence of preload on bearing dynamics

Smearing is adhesive wear and leads to premature bearing failure. High pressure and sliding of the contact surfaces lead to a high energy input into the surfaces (see Eq. 1), which results in material transfer and structural alterations [7]. High pressure combined with sliding of the rolling elements can be particularly prevalent in the acceleration zone of the rolling bearing [8]. Figure 1 shows the different zones of a rolling bearing and the corresponding rolling element speeds. Due to insufficient contact with the raceway in the deceleration zone as a result of too low loading outside the load zone, the rolling elements are slowed down by the frictional forces. When re-entering the load zone, the rolling elements pass through the acceleration zone, where there is still high slip while the pressure increases rapidly.

The deceleration zone can be minimized or completely avoided by a wider load zone [10]. For this purpose, TRBs can be preloaded, which generates a load component in axial and radial direction and ensures sufficient minimum load on the roller elements. Preload can be achieved by axially displacing the inner ring against the outer ring. Figure 2 shows the influence of the preload on the bearing load distribution. With a constant radial load F_{rad}, the width of the load zone increases with increasing preload until a 360° load zone prevails.

However, preload also affects the bearings overall behavior (e.g. lifetime). The influence is illustrated qualitatively in Fig. 3. The increased pressure due to the preload results in an increased frictional torque. Furthermore, preload increases the resulting bearing load during operation and

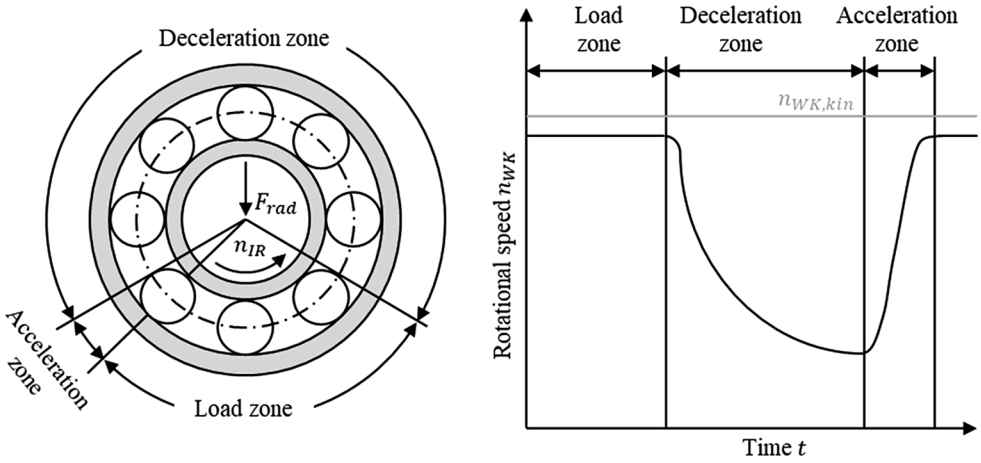

Fig. 1 Speed zones in rolling bearings. (According to [9])

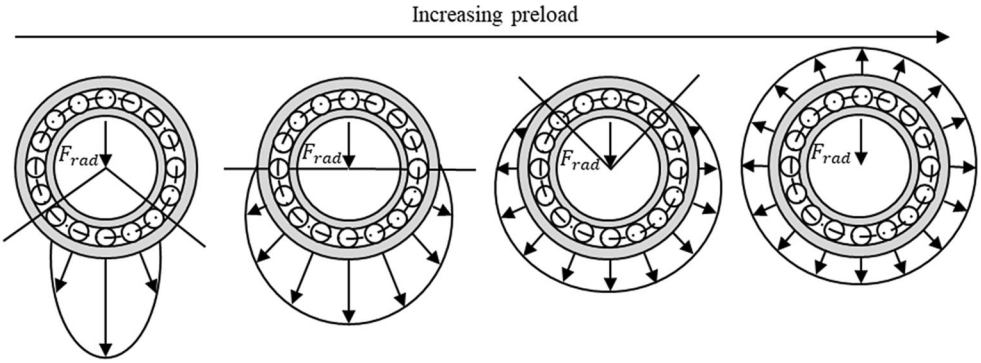

Fig. 2 Influence of axial preload on load distribution. (According to [11])

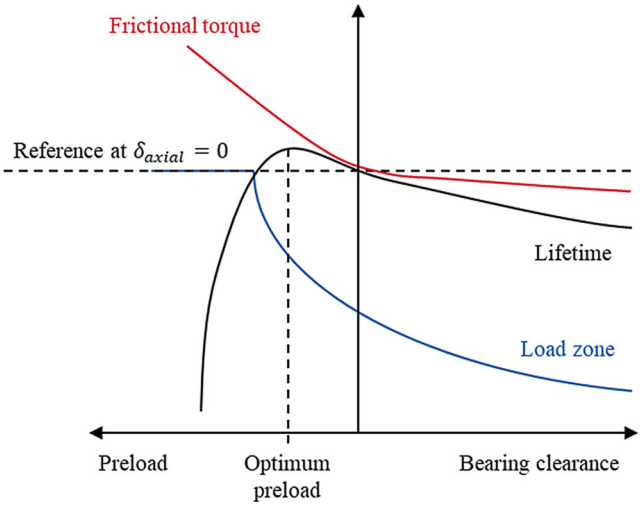

Fig. 3 Influence of preload on bearing dynamics and lifetime. (According to [12])

thus may reduce the service life. It is therefore essential to identify the optimal preload, which must balance the stated effects.

3 Approach

In this simulative investigation, the influence of grid faults on the smearing risk for TRBs on the HSS of a WT gearbox is determined. A validated multibody simulation (MBS) model of a 2.75 MW research nacelle is used for this purpose [13, 14]. The gearbox (see Fig. 4) is modeled using a flexible housing, flexible shafts, gear wheels including their microgeometry (e.g. tooth flank modifications) and bearings as spring-damper elements with stiffness curves provided by the bearing manufacturer.

The behaviour of the drivetrain in the event of a grid fault was investigated in detail in previous studies [6, 15]. This involved performing extended co-simulations of the mechanical (drivetrain) and electrical (generator, power converter, transformer, grid) domain. The resulting torque curves for the drive and generator shafts are used as input for the analysis in this paper.

In order to quantify the influence of the preload on the smearing risk, the axial bearing clearance of the TRBs is varied. The parameter range includes values from positive axial clearance to negative axial clearance, which results in preload. To calculate the risk of smearing damage different energetic values are available, e.g. the frictional power intensity (FPI), which is an indicator for the power P that is

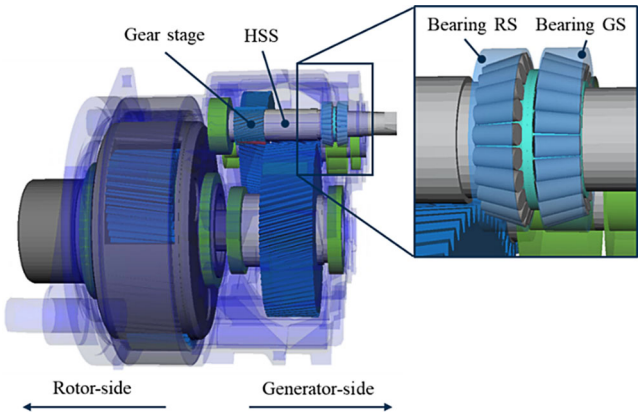

Fig. 4 MBS model of gearbox with detailed bearing models

introduced in the contact area A [8]. In this study, the FPI according to Eq. 1 is used.

$$FPI = \left(\frac{P}{A}\right)_{max} = \max\left(0.5 \cdot \mu\,(t) \cdot p_{\max(t)} \cdot \Delta u\,(t)\right) \quad (1)$$

The FPI is calculated using the coefficient of friction μ, the maximum pressure p_{max} and the relative speed of the contact partners Δu. To calculate these influencing factors, detailed contact models are necessary. Therefore, the gearbox model is extended with the bearing model LaMBDA at the investigated tapered roller bearings [16]. The geometry of the bearing as well as the lubricant properties are defined in Table 1.

It was shown in previous publications that LaMBDA can be used to calculate the risk of smearing damage [17]. The

Table 1 Bearing and lubrication data

Parameter	Value
Outer diameter	320 mm
Outer ring width	71 mm
Inner diameter	180 mm
Inner ring width	86 mm
Contact angle	15.699°
Roller element diameter	35 mm
Roller element width	74.9 mm
Roller element angle	4.339°
Number of roller elements	21
Oil viscosity class	ISO VG 320
Oil density	0.923 g/ml
Kinematic viscosity at 40 °C	317.57 cSt
Kinematic viscosity at 100 °C	36.44 cSt

contact calculation between rolling elements and rings is based on a discretized contact model in which the contact is divided into slices. It is based on the force-deformation relationship according to Tripp [18] and was extended by Teutsch to consider the mutual influence of the individual discs [19]. Each disc of rolling elements and rings is assigned a radius corresponding to the respective profile retraction [19]. Thus, the exact micro-geometry, in this case rollers and raceway profiling, can be considered. This is important for the pressure calculation, as the profiling is intended to reduce excessive pressure under unfavorable load situations, such as strong angular misalignments due to strong shaft deflection. With the contact normal force F_N per disc, which is calculated directly from the force-deformation relationship described, the pressure p is calculated using the following relationship in Eq. 2 with a and b being the semi-axes of an ellipse, which forms in the profiled contact between rolling elements and raceways.

$$p_i = \frac{F_{N,i}}{\pi \cdot a_i \cdot b_i} \quad (2)$$

The relative speed Δu is calculated for each contact and each disc according to Eq. 3. It is specified as the magnitude of the relative velocity vector at the contact point. The calculation is based on the difference between the velocities of the two bodies, rolling element and ring, projected onto the contact point.

$$\Delta u = \left|\vec{v}_{rel_i}\right| = \left|\vec{v}_{trans,RB_i} + \vec{v}_{rot,RB_i} - \vec{v}_{trans,R_i} - \vec{v}_{rot,R_i}\right| \quad (3)$$

$\vec{v}_{trans,RB_i}$ is the speed component from translational speed of rolling element at contact point, $\vec{v}_{rot,RB_i}$ from rotational speed of rolling element at contact point, $\vec{v}_{trans,R_i}$ from translational speed of ring at contact point and $\vec{v}_{rot,R_i}$ from rotational speed of ring at contact point.

The acceleration of the rolling elements at the beginning of the load zone and the deceleration outside the load zone depends heavily on the frictional losses. Therefore, the relative speed in contact Δu, can only be calculated reliably, if all frictional effects in the bearing are considered [20]. LaMBDA was validated against frictional torque measurements in several studies [16, 21, 22].

The friction coefficient μ of each contact point is determined according to Eq. 4 as the quotient of the tangential force in the contact F_T, which is the sum of all friction components acting at the contact point or, in other words, the sum of the traction forces, and the contact normal force F_N.

$$\mu_i = \frac{F_{T,i}}{F_{N,i}} \quad (4)$$

4 Results

In this section the simulation results are presented. First, the influence of grid faults on the smearing risk is discussed. Subsequently, the influence of bearing preload on the smearing risk in the event of a grid fault is quantified.

4.1 Smearing risk at grid faults

In order to evaluate the influence of grid faults on the smearing risk, the drive and generator torque curves during a grid fault measured in an experiment are used as an excitation for the simulative investigation in this paper. Figure 5 visualizes the two torque curves and the speed of the HSS. The data were normalized to the rated torque.

Initially, the drivetrain is accelerated to its rated speed using the rated drive torque. At t = 1.35 s, the generator torque is applied to the drivetrain. From this point onwards, the system is in rated operation. The grid fault occurs at t = 2 s. The generator torque rises abruptly to 2.15 times the rated torque and immediately begins to fluctuate. A linear reduction in drive torque is initiated 100 ms later, to account for the latency of the control and the pitch mechanism of WT in the field. During the grid fault, the speed of the HSS increases from 1100 rpm to a maximum of 1400 rpm. Given the high speed and the lower, oscillating load on the bearing, this condition is particularly critical for slippage in the bearings. From t = 2.5 s, the generator torque returns to a stable state, and from t = 3 s, the drive torque is increased to the rated torque. The system resumes rated operation after t = 4 s.

The influence of the grid fault on the smearing risk is illustrated in Fig. 6, which shows the maximum pressure p_{max}, the maximum sliding speed Δu and the resulting maximum FPI.

The results are presented for the rotor-side TRB RS and the generator-side TRB GS, as they show different bearing dynamics due to the external forces. In each case, the values

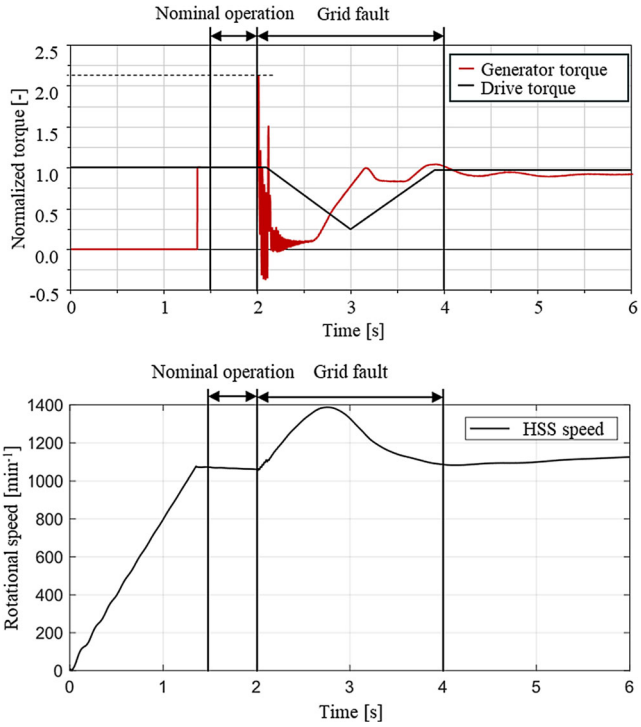

Fig. 5 Torque curves of the drive train (*top*) and HSS speed (*bottom*) during grid fault

of one rolling element are evaluated. The axial clearance is set to the reference value of δ = 0 µm. The key values of the simulation are presented in the following Table 2.

In rated operation, the maximum pressure is comparable for both bearings, but the sliding speed is greatly reduced for bearing GS, which is subjected to higher loads. This results in a lower FPI for bearing GS. The FPI increases significantly for both bearings in the event of a grid fault. The increase is primarily due to the elevated sliding speed, which has increased by 126% for bearing GS. Despite the slight reduction in the maximum pressure, there is therefore

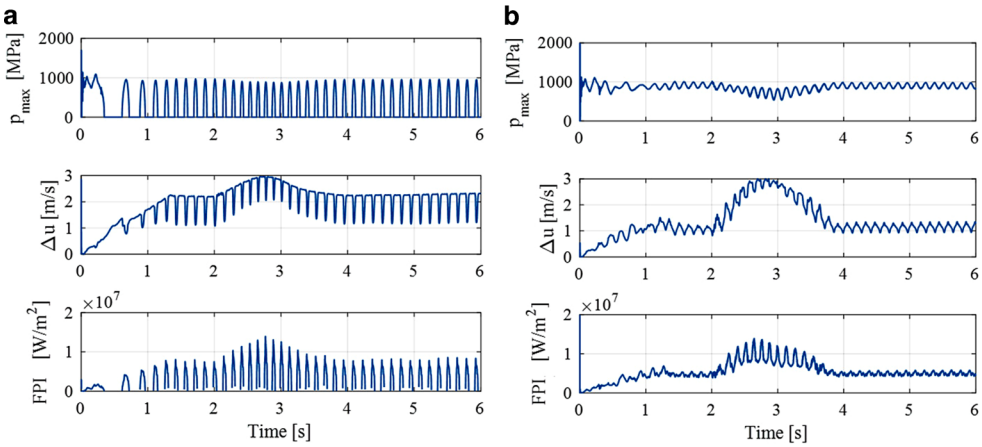

Fig. 6 Bearing dynamics and FPI during grid fault

Table 2 Comparison of FPI for both bearings during grid faults

Parameter	Bearing RS	Bearing GS
Max. pressure, rated operation $p_{max,ro}$	962 MPa	997 MPa
Max. pressure, grid fault $p_{max,gf}$	959 MPa	990 MPa
Max. sliding speed, rated operation Δu_{ro}	2.41 m/s	1.44 m/s
Max. sliding speed, grid fault Δu_{gf}	3.20 m/s	3.25 m/s
Max. FPI, rated operation FPI_{ro}	$8.15 \cdot 10^6$ W/m^2	$5.74 \cdot 10^6$ W/m^2
Max. FPI, grid fault FPI_{gf}	$14.05 \cdot 10^6$ W/m^2	$13.92 \cdot 10^6$ W/m^2

a significant increase in the FPI of 72% for bearing RS and 143% for bearing GS during the grid fault.

4.2 Influence of preload on smearing risk at grid faults

The following section discusses the influence of preload on the smearing risk of the TRBs in the event of grid faults. Figure 7 shows the resulting bearing dynamics and FPI for two different cases preloading cases. In the first case, an axial bearing clearance of δ = 200 µm was applied, while in the second case, a negative axial bearing clearance of δ = –200 µm was applied, resulting in preloading of the bearing. Typically, TRBs are operated with preload, however, thermal expansion and wear can cause the loss of preload or even axial clearance in the bearing arrangement [23, 24].

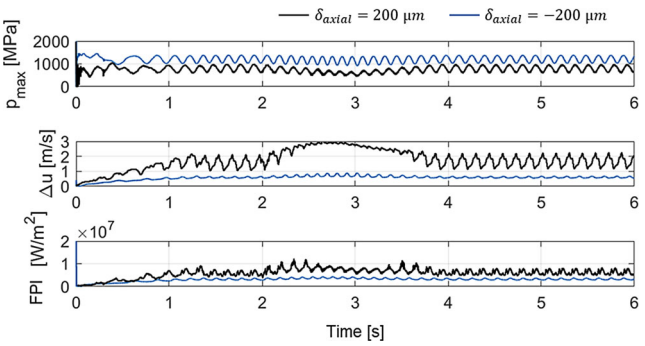

Fig. 7 Influence of preload on bearing dynamics and FPI during grid fault

Consequently, both the preload and the axial clearance are subject to analysis. In both cases, the TRB on the generator side is analyzed.

In rated operation, the preloaded bearing has a lower FPI, despite the higher maximum pressure. This is due to the lower sliding speed resulting from a wider load zone. During the grid fault, the FPI for the preloaded bearing remains almost constant. In comparison, the bearing with axial clearance exhibits a significant rise in FPI of 56%. This results from the elevated sliding speed, which is caused by the increased HSS speed and dynamic bearing loads resulting from the torque excitations. Since the changed kinematics in the bearing are the main driver for the FPI increase, it is crucial to analyze the sliding speed. Further Fig. 8 illustrates the maximum resulting sliding speed as a function of the axial clearance and preload for both bearings.

As expected, a reduction in the sliding speed can be observed with increasing preload. A prominent characteristic of bearing RS is the rise in sliding speed at an axial clearance of δ > 150 µm. From this point onwards, the sliding speed increases to a Δu = 14.35 m/s and remains almost constant even if the axial clearance is increased further. At this point, the rolling elements have almost no contact with the raceway. As a result, the rolling elements are no longer properly accelerated, which leads to very high sliding speeds. This behaviour can be further examined looking at the load distribution of the two bearings for varying axial clearances (see Fig. 9).

Fig. 8 Influence of axial preload and clearance on sliding speed

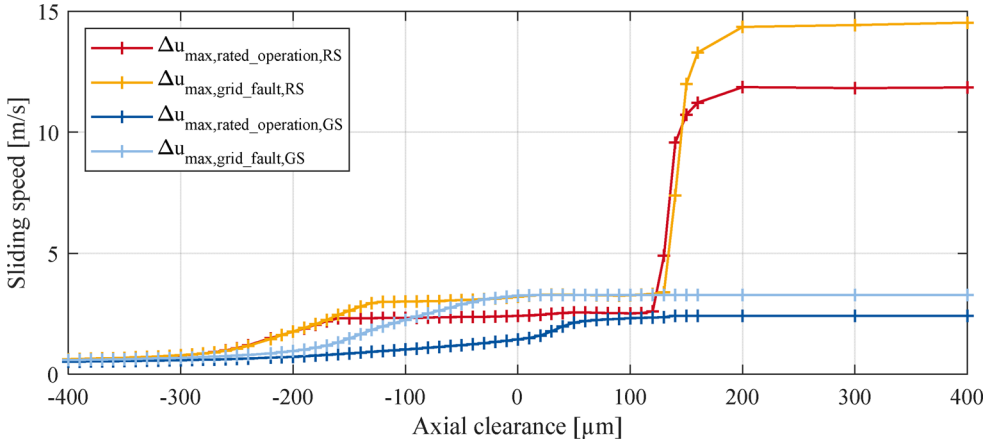

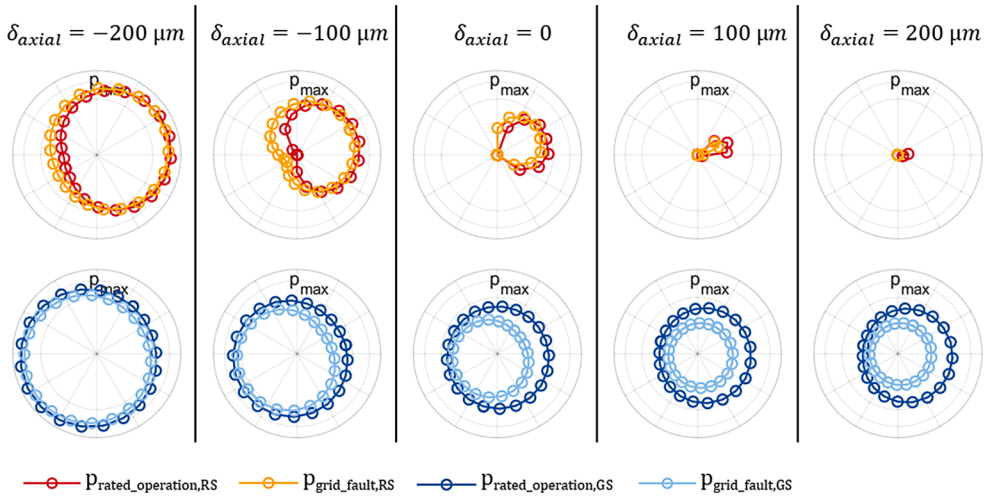

Fig. 9 Influence of axial preload and clearance on load distribution

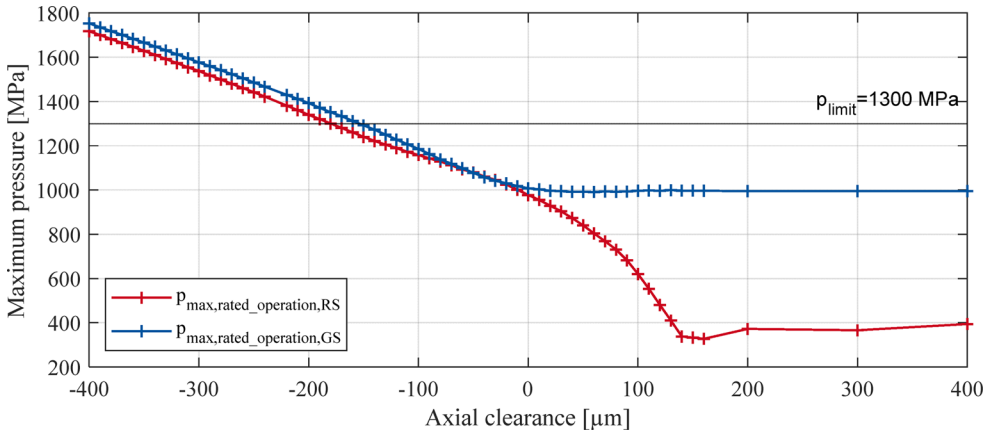

Fig. 10 Influence of axial preload and clearance on Hertzian pressure

The load distribution of the rotor-side bearing RS becomes increasingly uneven with increasing axial clearance. Also, the load distribution zone becomes smaller. A decrease in the maximum pressure is also observed in the generator-side bearing GS. However, a continuous load zone persists for bearing GS due to external forces.

The maximum pressure has a relatively minor impact on the FPI. Figure 10 illustrates the maximum pressure as a function of the axial clearance for both bearings. For an axial clearance of $\delta < 0\,\mu m$, resulting in preload, the maximum pressure is observed to be almost the same for both bearings. As the axial clearance increases, the maximum pressure goes down to $p_{max} = 994\,MPa$ for bearing GS, while the maximum pressure for bearing RS decreases to $p_{max} = 371\,MPa$.

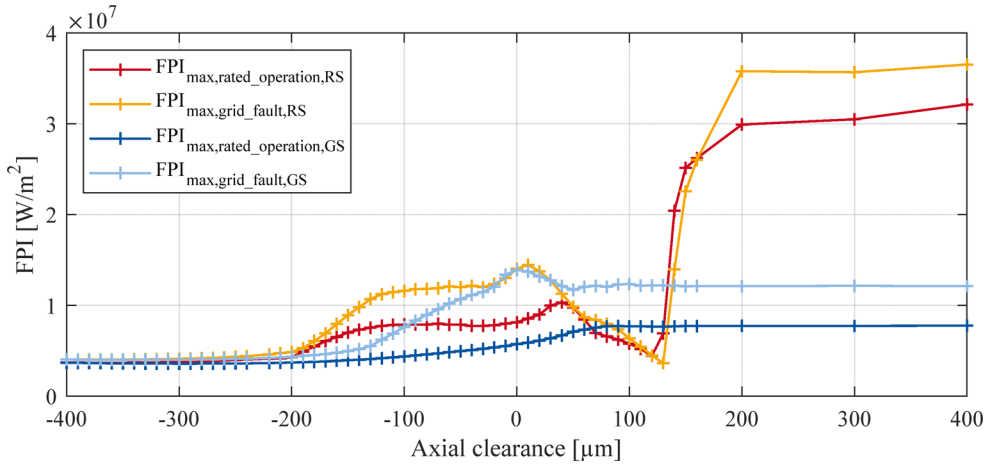

Fig. 11 Influence of axial preload and clearance on FPI

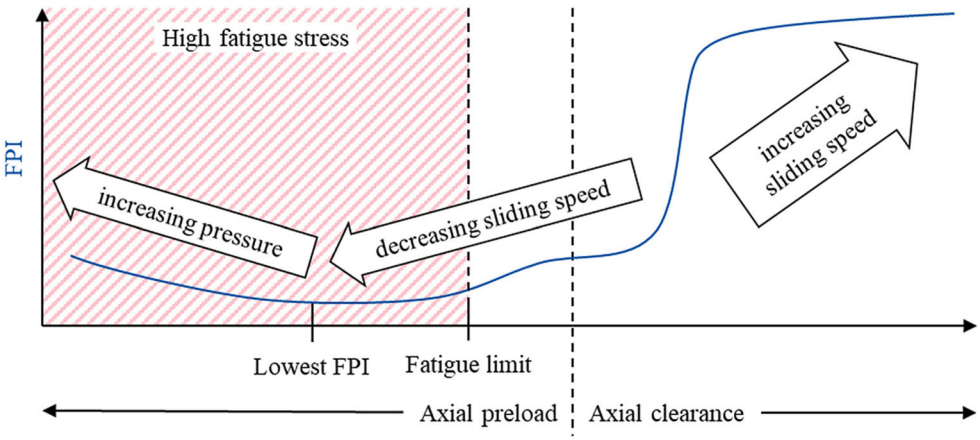

Fig. 12 Influence of axial preload and clearance on FPI

In general, an increase in preload results in a reduction in the FPI. Figure 11 illustrates the impact of axial clearance on the FPI.

The lowest FPI is achieved with an axial clearance of $\delta = -370\,\mu m$. However, at this point the fatigue limit pressure of the bearings is clearly exceeded (see Fig. 10). The limiting pressure is exceeded at a preload of $\delta > -160\,\mu m$. Considering the limiting pressure, the lowest FPI, for both rated operation and grid faults for bearing RS and GS, is achieved at an axial clearance of $\delta = -150\,\mu m$.

5 Conclusion

Rolling bearings in WT gearboxes often fail prematurely, causing downtime of the WTs. Especially the bearings on the HSS of the WT gearbox are prone to failure [2]. Critical conditions within the HSS bearings may result from significant torque excitations, which make the bearings prone to slip-induced damage, such as smearing [3]. Torque excitations are induced, among other things, by grid faults [4]. Therefore, in this paper the smearing risk during grid faults was examined simulatively for the TRBs on the HSS. In addition, the influence of preload on the smearing risk was quantified. For this purpose, a detailed model of the TRBs was integrated into the MBS model of a 2.75 MW research nacelle.

Subsequently, the smearing risk was evaluated using the FPI. It was shown that at a reference axial clearance of $\delta = 0\,\mu m$, the FPI increases by 72% for the rotor-side bearing and by 143% for the generator-side bearing in the event of a grid fault compared to rated operation. This is due to the high sliding speeds within the TRBs. Therefore, an increase in smearing risk is expected.

The sliding speeds can be reduced by increasing the preload to a reliable extent. The lowest FPI is achieved with an axial clearance of $\delta = -370\,\mu m$ with almost no increase during the grid fault. However, at this point, the fatigue lifetime of the bearings decreases significantly due to the high pressures resulting from the preload. Conversely, operating the TRBs with axial clearance, which may be caused by thermal expansion or wear, results in an increase in sliding speed.

Consequently, there has to be a multifactorial design optimization of the TRB arrangement and the different damage criteria to derive the optimal preload. The influence of the axial clearance and the conflict of objectives is shown qualitatively in Fig. 12. The optimal design is a trade-off between high fatigue lifetime and low FPI (area between high fatigue stress and 0 axial clearance).

Funding The authors thank the Ministry of Economic Affairs, Industry, Climate Action and Energy of the State of North Rhine-Westphalia, Germany, for the financial support granted. They also thank their project partners for the equipment, insight as well as expertise, which contributed to this joint project. The software LaMBDA used in this paper was developed in a research project funded by Arbeitsgemeinschaft industrieller Forschungsvereinigungen (AiF) e. V. and Forschungsvereinigung Antriebstechnik (FVA) e. V., FVA project number 625 III, grant number 20764 N.

Funding Open Access funding enabled and organized by Projekt DEAL.

References

1. Rohrig K et al (2019) Powering the 21st century by wind energy—Options, facts, figures. Appl Phys Rev 6:
2. Shuangwen S (2013) Report on wind turbine subsystem reliability: a survey of various databases. National Renewable Energy Laboratory (Presentation)
3. Sheng S (2016) Wind turbine gearbox reliability database, condition monitoring, and operation and maintenance research update
4. Röder J, Jacobs G, Duda T, Bosse D (2020) Simulative investigation of the load propagation in a wind turbine drive train during a power converter fault. Universitätsbibliothek der RWTH Aachen, Aachen
5. Euler J, Jacobs G, Röder J, Bosse D (2022) Simulative investigation of the risk of smearing damage for a WT gearbox roller bearing during rotor-induced excitations. Wind 2:348–356
6. Röder J, Jacobs G, Bosse D, Izal JLR (2022) Reduction of gearbox loads of a DFIG wind turbine during grid faults with optimized converter configurations. Universitätsbibliothek der RWTH Aachen, Aachen
7. Stuhler P, Nagler N (2021) Stand der Technik: Anschmierungen in Radial-Zylinderrollenlagern: Definition, Mechanismus, Einflüsse, Abhilfen und Potenziale. In: Forschung im Ingenieurwesen, pp 1–20
8. van Lier H (2016) Neuhärtungsgefährdung von Radial-Zylinderrollenlagem durch Lastaufschaltungen. Fakultät für Maschinenwesen, Rheinisch-Westfälischen Technischen Hochschule (Dissertation)
9. Fingerle T Experimentelle und simulative Untersuchung des Schlupfverhaltens von Kegelrollenlagern. Technische Universität Kaiserslautern (Dissertation)
10. Helsen J, Guo Y, Keller J, Guillaume P (2016) Experimental investigation of bearing slip in a wind turbine gearbox during a transient grid loss event. Wind Energy 19:2255–2269
11. Sommer K, Heinz R, Schöfer J (2018) Verschleiß metallischer Werkstoffe: Erscheinungsformen sicher beurteilen, 3rd edn. Springer, Wiesbaden
12. SKF Gruppe (2021) Wälzlager PUB BU/P1 17000/1 DE
13. Matzke D (2022) MKS-basierte Gesamtanlagenmodelle zur Lastrechnung für WEA-Getriebe. Fakultät für Maschinenwesen, Rheinisch-Westfälischen Technischen Hochschule (Dissertation)
14. Matzke D, Jacobs G, Schelenz R (2019) Validation of MBS modeling methods to calculate bearing andtooth loads in the planetary gear stage of a wind turbine
15. Röder J, Jacobs G, Duda T, Bosse D, Herzog F (2021) Investigation of dynamic loads in wind turbine drive trains Due to grid and power converter faults. Energies 14:8542
16. Wingertszahn P, Graf S, Koch O (2023) Dynamikmodelle verschiedener Wälzlagertypen: Betriebsverhalten von Kegelrollenlagern in Abhängigkeit der Belastungssituation im Antriebssystem. Forschungsvereinigung Antriebstechnik e. V., Frankfurt/Main
17. Wingertszahn P, Koch O (2024) Prediction of bearing damage beyond rolling contact fatigue. 78th Annual Meeting & Exhibition (STLE) 2024, Minneapolis
18. Tripp JH (1983) Surface roughness effects in hydrodynamic lubrication: the flow factor method. J Lubr Technol 105:458–463
19. Teutsch R, Sauer B (2004) An alternative slicing technique to consider pressure concentrations in non-hertzian line contacts. J Tribol 126:436–442
20. Wingertszahn P, Koch O (2024) Vorhersage von Lagerschäden jenseits von Rolling Contact Fatigue. 6. VDI-Fachkonferenz Schadensmechanismen an Lagern, Aachen
21. Wingertszahn P, Koch O, Maccioni L, Concli F, Sauer B (2023) Predicting friction of tapered roller bearings with detailed multibody simulation models. Lubricants 11:369
22. Wingertszahn P, Koch O (2023) Prediction of friction torque and kinematics of tapered roller bearings with detailed multibody simulation. 4th International Brazilian Conference on Tribology—TriBoBR 2023, Vitoria-ES
23. Hotta T, Noguchi S, Kanada T (2016) Fundamental study on preload loss in tapered roller bearings. Tribol Online 11:326–332
24. Jain A, Singh A, Singh AP (2019) Effect of tribological parameters on sliding wear and friction coefficient which relates to preload loss in tapered roller bearing. ILT 71:61–73